

DUST PROPERTIES OF [C II]–DETECTED $Z \sim 5.5$ GALAXIES: NEW HST/WFC3 NEAR-IR OBSERVATIONS

IVANA BARIŠIĆ^{1,2}, ANDREAS L. FAISST³, PETER L. CAPAK³, RICCARDO PAVESI⁴, DOMINIK A. RIECHERS⁴, NICK Z. SCOVILLE⁵, KEVIN C. COOKE⁶, JEYHAN S. KARTALTEPE⁶, CAITLIN M. CASEY⁷, VERNESA SMOLČIĆ¹

¹Department of Physics, Faculty of Science, University of Zagreb, Bijenička cesta 32, 10000 Zagreb, Croatia

²Max-Planck Institut für Astronomie, Königstuhl 17, D-69117, Heidelberg, Germany

³Infrared Processing and Analysis Center, California Institute of Technology, Pasadena, CA 91125, USA

⁴Department of Astronomy, Cornell University, Space Sciences Building, Ithaca, NY 14853, USA

⁵Cahill Center for Astronomy and Astrophysics, California Institute of Technology, Pasadena, CA 91125, USA

⁶School of Physics and Astronomy, Rochester Institute of Technology, 84 Lomb Memorial Drive, Rochester, NY 14623, USA

and

⁷Department of Astronomy, The University of Texas at Austin, 2515 Speedway Blvd Stop C1400, Austin, TX 78712, USA

ABSTRACT

We examine the rest-frame ultra-violet (UV) properties of 10 [C II] $\lambda 158\mu\text{m}$ –detected galaxies at $z \sim 5.5$ in COSMOS using new HST/WFC3 near-infrared imaging. Together with pre-existing $158\mu\text{m}$ –continuum and [C II] line measurements by ALMA, we study their dust attenuation properties on the IRX– β diagram, which connects the total dust emission ($\propto \text{IRX} = \log(L_{\text{FIR}}/L_{1600})$) to the line-of-sight dust column ($\propto \beta$). We find systematically bluer UV continuum spectral slopes (β) compared to previous low-resolution ground-based measurements, which relieves some of the tension between models of dust attenuation and observations at high redshifts. While most of the galaxies are consistent with local starburst or Small Magellanic cloud like dust properties, we find galaxies with low IRX values and a large range in β that cannot be explained by models of a uniform dust distribution well mixed with stars. A stacking analysis of Keck/DEIMOS optical spectra indicates that these galaxies are metal-poor with young stellar populations which could significantly alter their spatial dust distribution.

Keywords: galaxies: ISM — dust, extinction — galaxies: formation — galaxies: evolution — galaxies: ISM — galaxies: high-redshift

1. INTRODUCTION

Galaxies at $z > 4$ likely have different inter-stellar medium (ISM) properties than galaxies in the local Universe (e.g., Carilli & Walter 2013). For example, studies of emission line ratios of high redshift ($z > 4$) galaxies by Spitzer suggest that early galaxies grow at a fast pace,

with high specific star-formation rates (SFR) and stellar mass assembly time scales of only a couple of 100 Myrs (de Barros et al. 2014; Faisst et al. 2016a; Jiang et al. 2016). A substantially higher gas fraction as well as changes in the ionization parameter of stellar radiation indicated by the [O III]/[O II] line ratio are also observed, indicative of a different H₂ region configuration (Steidel et al. 2014; Genzel et al. 2015; Silverman et al. 2015; Scoville et al. 2016; Faisst 2016; Masters et al. 2016).

So far, direct studies of the ISM at $z > 4$ have been

difficult due to the lack of sensitivity in the far-infrared (FIR) and sub-millimeter (sub-mm) wavelengths where the key ISM diagnostics are present. With the *Atacama Large Millimeter/Sub-millimeter Array* (ALMA) it is now possible to study the ISM of galaxies at very high redshifts via the measurement of the [C II] $158\ \mu\text{m}$ emission and the FIR continuum. Some of the first studies of $z > 4$ galaxies with ALMA find significantly lower dust continuum emission than those found in local galaxies (Riechers et al. 2014; Capak et al. 2015; Maiolino et al. 2015; Schaerer et al. 2015; Watson et al. 2015; Bouwens et al. 2016; Carilli et al. 2016; Dunlop et al. 2017; Knudsen et al. 2016).

Studying a sample of 10 Lyman Break Galaxies (LBGs) at $5 < z < 6$, Capak et al. (2015) (hereafter C15) find the ratio of infrared to ultraviolet light ($L_{\text{FIR}}/L_{1600} = \text{IRX}$) at a given UV continuum spectral slope (β) in the so-called IRX– β relation to be significantly lower than what was expected from dust attenuation models (e.g., Charlot & Fall 2000) or even in local low-metallicity galaxies like the Small Magellanic Cloud (SMC, Pettini et al. 1998). Furthermore, there are galaxies with exceptionally red β slopes at low IRX values, which are difficult to physically explain (Charlot & Fall 2000). These findings are curious and, if confirmed, would imply a substantial evolution of ISM properties in the first 1 billion years of the Universe. These measurements leave significant uncertainty in what is physically occurring. First, the FIR luminosities are derived from a single ALMA continuum point at rest-frame $158\ \mu\text{m}$, which means significant assumptions on the shape of the FIR spectral energy distribution (SED) must be made. Second, the β measurements are derived from low signal-to-noise (S/N) ground-based data, which results in significant systematic uncertainty (e.g., Dunlop et al. 2012; Rogers et al. 2013).

In this letter, we present deep *Hubble Space Telescope* (HST) near-IR imaging to provide improved measurements of β and the UV luminosity (L_{1600}) for the 10 originally targeted, two serendipitous sources, and two sub-components of one of the galaxies that are resolved by HST at $z \sim 5.5$ presented in C15 (Section 2). We carefully investigate potential systematics in the derivation of these parameters by performing extensive simulations to eventually pinpoint the location of these galaxies on the IRX– β plane (Sections 3 and 4). A companion paper (Faisst et al., in prep) presents an additional analysis of the dust temperatures and far-infrared properties of these galaxies given a sample of local galaxies.

We assume a flat cosmology with $\Omega_{\Lambda,0} = 0.7$, $\Omega_{m,0} = 0.3$, and $h = 0.7$. Magnitudes are quoted in AB (Oke 1974).

2. DATA

2.1. Sample selection and auxiliary data

The sample that is used in this work is based on C15 and we describe its properties in brief in the following. The sample consists of 9 star-forming LBGs at 1 – 4 times the characteristic luminosity (L^*) and one low luminosity quasar *HZ5*, see Capak et al. (2011) observed at $5 < z < 6$ in the 2 square-degree field of the *Cosmic Evolution Survey* (COSMOS, Scoville et al. 2007)¹, which provides a multitude of photometric data (Laigle et al. 2016). Note that we will not use *HZ5* in the following analysis of this work. The sample is initially selected by a range of techniques and designed to be representative of $z = 5 - 6$ galaxies in many quantities including SFR, stellar mass, and metallicity. The ten objects are followed up with the *Deep Extragalactic Imaging Multi-Object Spectrograph* (DEIMOS, Faber et al. 2003) to spectroscopically confirm their redshifts via the rest-frame UV absorption features. Out of ten galaxies, six show a strong Ly α emission while three show only weak emission. No Ly α was detected in *HZ3*. The galaxies cover a large range in SFRs and stellar masses (see C15) and the UV absorption features suggest gas-phase metallicities of $12 + \log(\text{O}/\text{H}) = 8.0 - 8.5$, representative of the average metallicity of $\log(M/M_{\odot}) \sim 10$ galaxies at $z \sim 5$ (Faisst et al. 2016b). The galaxies were observed with ALMA² targeting the wavelength around rest-frame $158\ \mu\text{m}$ including the FIR continuum and the [C II] emission line (Capak et al. 2015). All galaxies were detected in [C II] and four of them have detected FIR continuum. In addition, two serendipitously detected [C II] emitters (*HZ5a* and *HZ8W*) were found at the same [C II] redshift of *HZ5* and *HZ8* at a projected distance of 10 – 15 kpc and *HZ6* breaks into three sub-components for a total of 14 objects (Figure 1).

2.2. New HST/WFC3 observations

To study the rest-frame UV properties of these galaxies, we have obtained HST Wide Field Camera 3 (WFC3) imaging between March and July 2015 (HST Cycle 22, ID 13641, PI: P. L. Capak) in F105W, F125W, and F160W corresponding to $1.05\ \mu\text{m}$, $1.25\ \mu\text{m}$, and $1.54\ \mu\text{m}$, respectively. The ten galaxies were observed in ten separate pointings for one orbit per filter reaching 26.2, 26.4, and 25.9 AB (5σ in $1''$ aperture). Note that *HZ6* was observed in another HST program (HST Cycle 21, ID 13384, PI: D. Riechers) to which we added F105W. The standard HST data reduction procedure as explained in the HST Data Hand-

¹ <http://cosmos.astro.caltech.edu>

² ALMA Cycle 1, ADS/JAO.ALMA#2012.1.00523.S, PI: P. L. Capak. See C15 for a detailed description of this data.

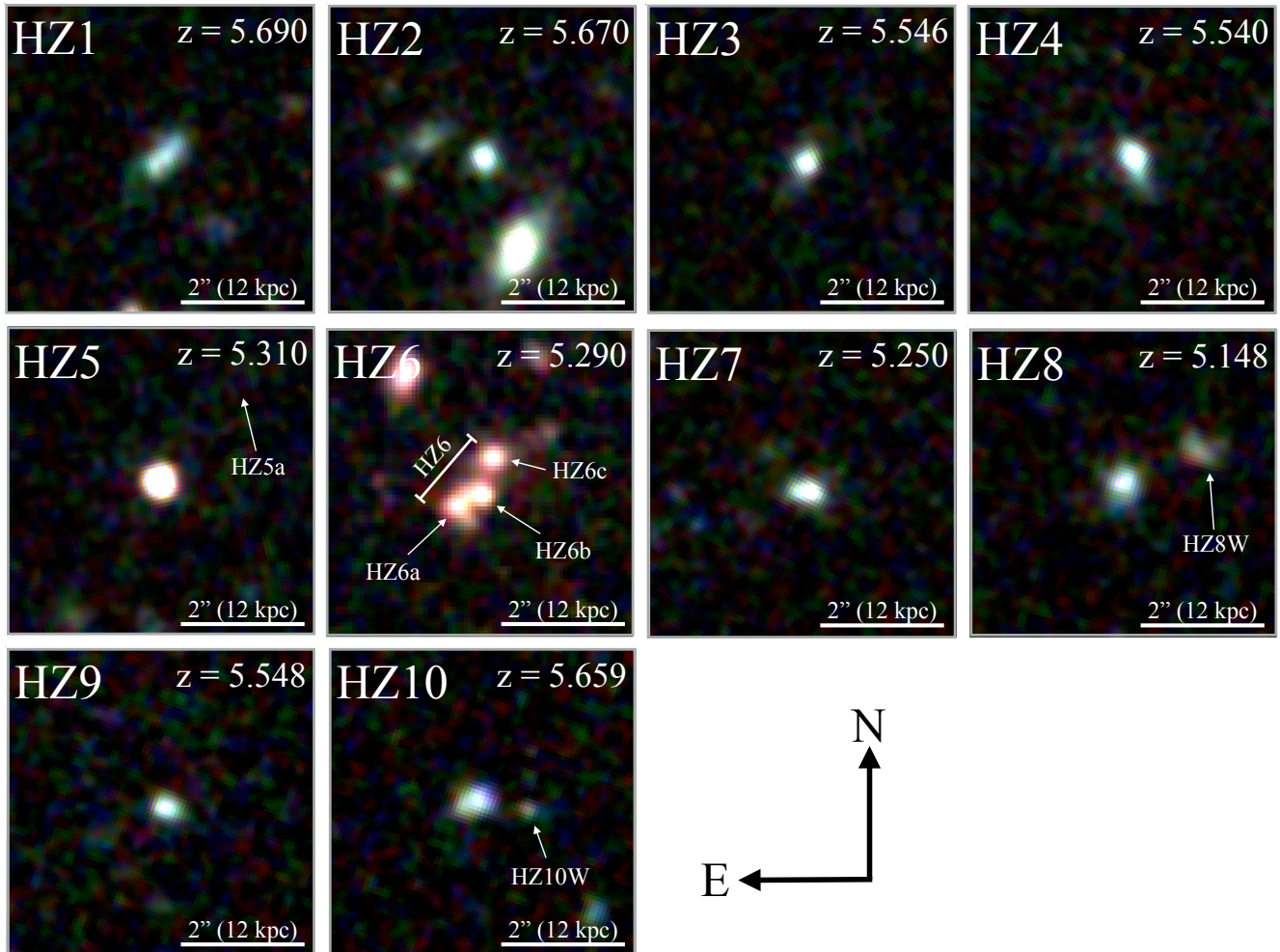


Figure 1. HST/WFC3 color (F105W (blue), F125W (green), F160W (red)) cut-outs from the 10 pointings. The two serendipitous [C II] detections HZ5a and HZ8W and other sub-components are indicated by white arrows.

book³ was used to convert the raw data frames into the final flat-fielded and flux-calibrated science products. Thereby we used the Pyraf/STSDAS calfw3 task to create a bad pixel array and to perform the bias and dark current subtraction of the read-outs. Geometric distortions have been corrected for using the latest distortion solutions (March 22 2012) provided by the STScI/WFC3 web-page and the exposures are joined using the Pyraf/STSDAS AstroDrizzle task. We use the HST/ACS F814W images available on the COSMOS field for the astrometric alignment of the frames to reach sub-arcsecond precision (Cooke et al. in prep). Figure 1 shows HST/WFC3 3-color cut-outs of each of the 10 pointings.

3. MEASUREMENTS & SIMULATIONS

The UV continuum slope β for star forming galaxies at high- z is dominated by the line-of-sight dust column density, which attenuates the UV light of the star forming regions⁴. It is therefore a valid tool to study the ISM column density of galaxies (Meurer et al. 1999; Kong et al. 2004; Casey et al. 2014). Furthermore, β is the only estimate of the dust content available for the vast majority of galaxies at $z > 3$ due to the relative insensitivity of contemporary optical and IR surveys. The β can be combined with IRX, which is sensitive to the total amount of dust, to form the IRX- β relation which can be used to infer the evolution of ISM properties.

The measurement of β at high redshifts is not trivial due to the scarcity of photometric bands covering

³ <http://www.stsci.edu/hst/wfc3/analysis>

⁴ Note that β also depends on internal properties of a galaxy such as the age and metallicity of a stellar population as well as its star-formation history. However, these affect less the overall β at high redshifts as compared to dust (see figure 13 in Bouwens et al. 2012)

the rest-frame UV part of the galaxies’ SEDs and low sensitivity from the ground. Furthermore, the measurement of β is particularly sensitive to the signal-to-noise of photometry and systematics in flux measurements, such as confusion from neighboring sources, background subtraction, and surface brightness effects (e.g., [Finkelstein et al. 2012](#); [Dunlop et al. 2012](#); [Rogers et al. 2013](#); [Bouwens et al. 2014](#)). High S/N data accompanied by simulations are therefore essential to correct for these effects. In the following sections we describe the measurement of the β and the methods used to access and correct systematic uncertainties.

3.1. Flux extraction and measurement of β

We use *Source Extractor* (version 2.5.0, [Bertin & Arnouts 1996](#)) to measure the fluxes of the galaxies in F105W, F125W, and F160W. For each of the galaxies, we manually tune the *Source Extractor*’s input parameters in order to optimize the de-blending, object detection, and background subtraction. The fluxes are measured in different aperture types including ISO, AUTO, as well as three manual apertures with radii $r = 0.8''$, $0.9''$, and $1.0''$. The isophotal flux threshold was set to 2σ relative to the weight map and the AUTO apertures use a minimum radius of 3.5 pixels ($0.45''$) for low S/N sources. We choose the Kron-factor (2.5) and the minimum radius (3.5px) to be the same for all pointings and wavelengths. From our realistic and extensive simulations (Figure 2, described in Section 3.2), we find that we can recover the AUTO magnitudes better than 0.05 mag down to 25AB magnitude. The simulations and visual inspection of the output photometry show that the AUTO magnitudes have the least systematic biases compared to other methods of measuring the photometry of the galaxies.

In addition to these main measurements, the near-IR HST photometry of the sub-components of *HZ6* are extracted using GALFIT (version 3.0.5, [Peng et al. 2010](#)) and additionally verified by manual apertures (agreement to better than 0.1 mag). The FIR [C II] line emission and $158\ \mu\text{m}$ continuum fluxes at the positions of the three sub-components are fitted by Gaussians with the size of the ALMA beam ($\sim 0.5''$). *HZ6a* and *HZ6b* are significantly blended with ALMA and therefore the relative flux extraction is uncertain by up to a factor of three depending on the weighting.

The UV spectral slopes of the galaxies are measured directly from the F105W, F125W, and F160W photometric bands, which correspond to rest-frame 1600 Å to 2400 Å at $z \sim 5.5$. We note that the effective center wavelength of the filters changes with the power-law function $f_\lambda \propto \lambda^\beta$ and must be accounted for in the measurement of β , since the filter transmission curves have a finite width and a calibration on the AB system assumes $\beta = -2$. We therefore use a forward-modeling approach to measure β for our galaxies. From a tightly spaced grid in intrinsic spectral slopes (β_{in}) and intercepts (C), we create power-law SEDs according to $\log(f_\lambda) = \beta_{in} \times \log(\lambda) + C$, which we convolve with the three filter transmission curves for F105W, F125W, and F160W, respectively. The best β_{in} is then found via χ^2 – minimization from the comparison of the previously obtained model fluxes and the measured fluxes of the galaxies. We obtain estimates of the measurement uncertainties on β by repeating the above steps and thereby varying the observed fluxes within their errors (assuming a Gaussian error distribution). In addition we add a 0.007 magnitude error coming from the uncertainties in the WFC3-IR detector chain calibration (S. Deustua, WFC3 team, private comm). The extracted photometry of the galaxies as well as the final β and L_{1600} with 1σ uncertainties are listed in Table 1.

Table 1. Summary of HST ultra-violet and ALMA FIR measurements for the C15 sample

ID	redshift	HST based measurements (this work)					ALMA FIR measurements ^a		
		F105W ^h	F125W ^h	F160W ^h	β	$\log(L_{1600}/L_\odot)$	$\log(L_{\text{FIR}}/L_\odot)$	$\log(L_{\text{CII}}/L_\odot)$	
HZ1	5.690	24.53 ± 0.04	24.31 ± 0.03	24.52 ± 0.05	$-1.92^{+0.14}_{-0.11}$	11.21 ± 0.01	< 10.32	8.40 ± 0.32	
HZ2	5.670	24.65 ± 0.03	24.50 ± 0.03	24.63 ± 0.05	$-1.82^{+0.10}_{-0.10}$	11.15 ± 0.01	< 10.30	8.56 ± 0.41	
HZ3	5.546	24.74 ± 0.04	24.57 ± 0.03	24.63 ± 0.04	$-1.72^{+0.12}_{-0.15}$	11.08 ± 0.01	< 10.53	8.67 ± 0.28	
HZ4	5.540	24.17 ± 0.02	24.21 ± 0.02	24.20 ± 0.03	$-2.06^{+0.13}_{-0.15}$	11.28 ± 0.01	11.13 ± 0.54	8.98 ± 0.22	
HZ5	5.310	23.48 ± 0.01	23.53 ± 0.01	23.12 ± 0.01	$-1.01^{+0.06}_{-0.12}$	11.45 ± 0.01	< 10.30	< 7.20	
HZ5a	5.310	$> 26.24^b$	$> 26.35^b$	$> 25.89^b$...	$< 10.37^b$	< 10.30	8.15 ± 0.27	
HZ6 (total) ^c	5.290	23.62 ± 0.03	23.45 ± 0.04	23.29 ± 0.03	$-1.14^{+0.12}_{-0.14}$	11.47 ± 0.10	11.13 ± 0.23^c	9.23 ± 0.04^c	
· HZ6a ^d		25.28 ± 0.36	24.90 ± 0.30	24.67 ± 0.25	$-0.59^{+1.05}_{-1.12}$	11.11 ± 0.07	10.26 ± 0.23^d	$8.32 \pm 0.06^{d,e}$	
· HZ6b ^d		24.77 ± 0.28	24.65 ± 0.33	24.58 ± 0.37	$-1.50^{+1.05}_{-1.22}$	11.00 ± 0.07	10.87 ± 0.23^d	$8.81 \pm 0.02^{d,e}$	
· HZ6c ^d		24.53 ± 0.16	24.43 ± 0.13	24.25 ± 0.10	$-1.30^{+0.51}_{-0.37}$	10.81 ± 0.07	10.79 ± 0.23^d	8.65 ± 0.03^d	

Table 1 continued

Table 1 (*continued*)

ID	redshift	HST based measurements (this work)					ALMA FIR measurements ^a		
		F105W ^h	F125W ^h	F160W ^h	β	$\log(L_{1600}/L_{\odot})$	$\log(L_{\text{FIR}}/L_{\odot})$	$\log(L_{\text{CII}}/L_{\odot})$	
HZ7	5.250	24.56 ± 0.04	24.42 ± 0.03	24.30 ± 0.03	-1.39 ^{+0.15} _{-0.17}	11.05 ± 0.02	< 10.35	8.74 ± 0.24	
HZ8	5.148	24.51 ± 0.04	24.37 ± 0.04	24.28 ± 0.04	-1.42 ^{+0.19} _{-0.18}	11.04 ± 0.02	< 10.26	8.41 ± 0.18	
HZ8W	5.148	25.68 ± 0.11	25.14 ± 0.07	24.88 ± 0.08	-0.10 ^{+0.29} _{-0.29}	10.57 ± 0.04	< 10.26	8.31 ± 0.23	
HZ9	5.548	24.99 ± 0.06	24.91 ± 0.05	24.83 ± 0.07	-1.59 ^{+0.22} _{-0.23}	10.95 ± 0.02	11.54 ± 0.19	9.21 ± 0.09	
HZ10	5.659	24.56 ± 0.05	24.48 ± 0.05	24.52 ± 0.06	-1.92 ^{+0.24} _{-0.17}	11.14 ± 0.02	11.94 ± 0.08	(9.60 ± 0.13) ^f	
· HZ10W ^g		26.83 ± 0.16	26.86 ± 0.13	26.63 ± 0.15	-1.47 ^{+0.77} _{-0.44}	10.23 ± 0.05	(11.64 ± 0.08) ^g	(8.93 ± 0.13) ^g	

^a Measurements by C15 unless noted differently. The FIR luminosity is integrated between $3\mu\text{m}$ and $1100\mu\text{m}$.

^b 5σ limits in $1''$ aperture.

^c Integrated photometry of all the sub-components. We use the ALMA data: ADS/JAO.ALMA# 2011.0.00064.S (Riechers et al. 2014; Pavesi et al. 2016).

^d The photometry for the sub-components of HZ6 is measured by GALFIT. The ALMA properties are re-extracted using the F160W data as spatial prior.

^e The quoted uncertainties are formal fitting uncertainties. The actual uncertainties for HZ6a and HZ6b are larger (up to 0.2dec) due to severe blending.

^f Updated value from Pavesi et al. (2016).

^g Photometry measured in a $0.5''$ aperture. We assume half the FIR and [C II] luminosity of HZ10.

^h The quoted errors are measurement noise. For computing β we have added 0.007 mag of systematic uncertainty due to the WFC3-IR detector chain calibration (S. Deustua, WFC3 team, private comm). The systematic noise due to the photometry method is included in the simulations. The conversion of WFC3-IR fluxes to the absolute frame is uncertain at the 2.1% level, but is dominated by the uncertainty of the standard star system which does not affect the measured colors.

3.2. Simulations

We now assess possible systematic uncertainties of our β measurements arising from biases in the extraction of the photometry. For this, we create model galaxies, which are placed onto the original HST pointings and re-extracted with the same parameters used for the real galaxies. Following our approach in Section 3.1, we create 1,000 random model SEDs with $-3 < \beta < 2$ and $22 < \text{mag}_{\text{F160W}} < 26$ from which we obtain F105W, F125W, and F160W total fluxes by convolving with the respective filter transmission curves. The actual model galaxies are parametrized by a 2-dimensional Gaussian light distribution scaled to their total fluxes in each filter and with half-light sizes equal to the median measured for the real galaxies in the respective filters ($\sim 0.17''$). The model galaxies are then placed randomly in empty spots on each of the 10 HST calibrated pointings. For this we stack the segmentation images in all three filters as returned by *Source Extractor* and require a box of 20×20 pixels of clean sky background around the coordinate at which the model galaxies is inserted onto the frame. The model galaxies are re-extracted and analyzed in the same way as the real galaxies in order to obtain their output fluxes and spectral slope (β_{out}).

Figure 2 shows the results of our simulations. Each of the 10 panels in the top figure correspond to one

HST pointing and shows the difference $\beta_{\text{out}} - \beta_{\text{in}}$ as a function of output F160W magnitude. The observed magnitude of the 10 galaxies in each frame including the two serendipitous [C II] detections is indicated with blue lines. The increase in scatter for fainter magnitudes (i.e., lower S/N) is clearly visible. For brighter magnitudes we find a fast convergence to $\beta_{\text{out}} - \beta_{\text{in}} = 0$ as expected. In general, we find systematic offsets in our β measurements of less than $\Delta\beta = 0.05$ at the observed magnitudes of our galaxies, which is several factors less than the actual measurement uncertainties. We therefore conclude that our β measurements are robust and not significantly biased. We also note that the scatter from the true β seen in the simulation is consistent with the 1σ uncertainty we derive for the β measurements (see Table 1), which suggests that the dominant factor of uncertainty is photometric and a power-law approximation for the galaxies' SEDs is reasonable. We do not find significant biases (< 0.05 mag up to 25.5 AB) in recovering the AUTO magnitudes (lower panel in Figure 2). Finally, we note that our simulations show that the photometry computed in ISO and manual ($1''$) apertures are systematically biased at > 24.5 AB by 0.1 mag and 0.15 mag, respectively, due to surface brightness effects. Such β values would therefore be substantially biased, so we are using the AUTO magnitude based β

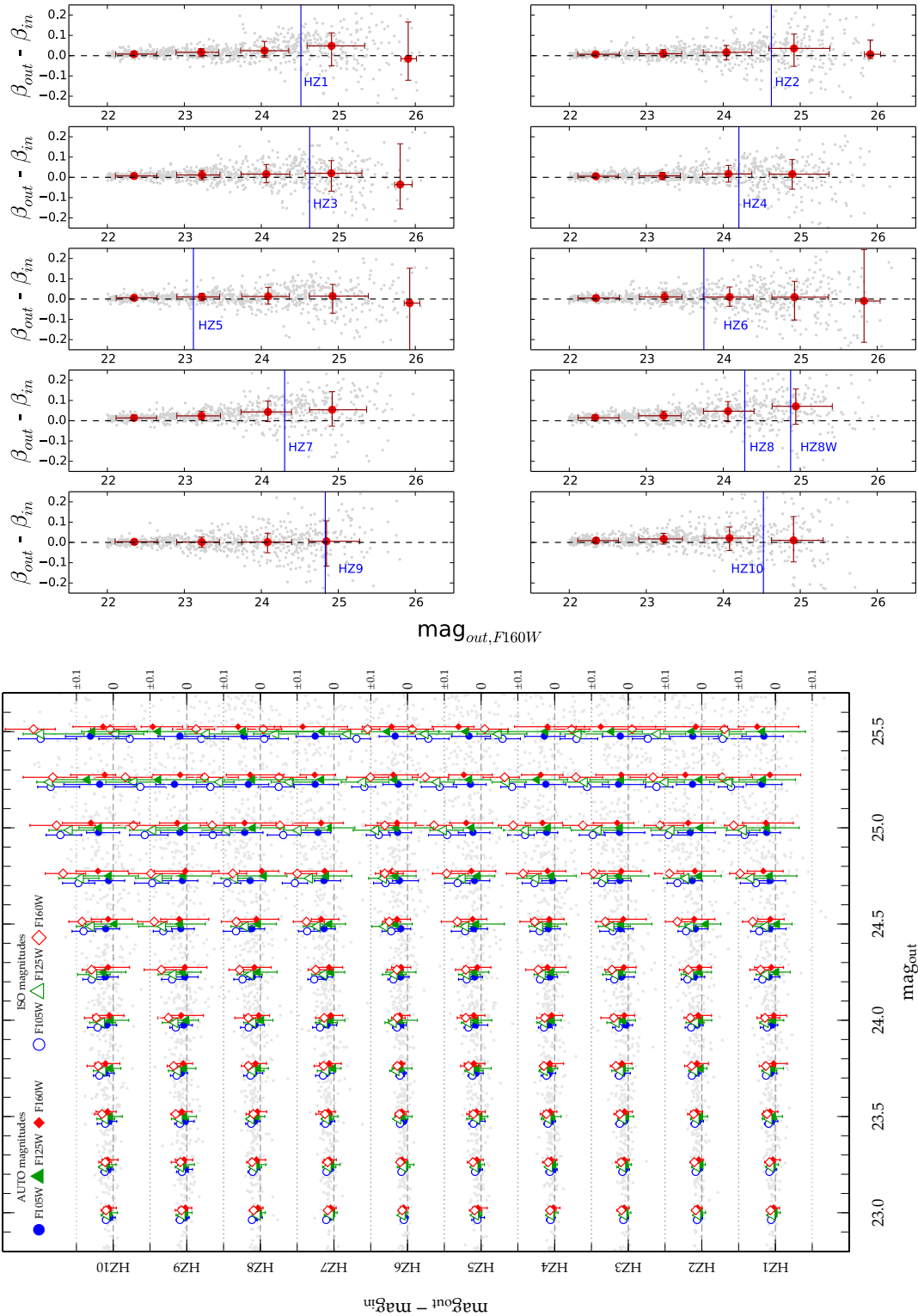


Figure 2. Results from our simulations. *Top:* Recovering error of β as a function of output F160W magnitude for each HST pointing (gray for single galaxies, red in bins of magnitude). The simulation suggests no significant biases. *Bottom:* Recovering error in F105W (blue dots), F125W (green triangles), and F160W (red diamonds) magnitudes for the ten HST pointings (filled: AUTO magnitude; open: ISO magnitudes). ISO magnitudes deviate systematically from the true by more than 0.1 mag at > 24.5 AB in comparison to AUTO magnitudes (< 0.1 mag up to 25.5 AB).

measurements here.

4. RESULTS & DISCUSSION

The upper left panel of Figure 3 shows the updated location of the galaxies in blue. The UV luminosities of our study and C15 are in good agreement within the errors. Our new HST based β measurements are consistent within errors with C15, but we find a systematic bias of the previous ground-based data toward redder slopes. This is due to the low S/N and systematic uncertainties of that data as noted by C15 which add a 0.3 dex systematic error bar on their measurements. Importantly, we have pinned down the β of the $z \sim 5.5$ galaxies with our new observations with sufficient precision and accuracy to make quantitative statements about the evolution of the IRX– β relation. We find that roughly 2/3 of the galaxies are consistent with the dust attenuation models of local starbursts or the SMC extinction law. However, 1/3 consists of low IRX objects residing *below* the SMC curve with a large range in β . The redder UV colors could be explained by dust-poor post-starburst galaxies with old stellar populations. However, the Spitzer colors suggesting substantial H α emission, as well as the spectroscopically confirmed strong Ly α line emission, are indicative of young stellar populations for these galaxies (see below). Instead, these galaxies are suggested to have a significant dust attenuation along the line-of-sight, while their low IRX values indicate only very little radiation in the IR, i.e., an overall low dust mass. This is at odds with SMC dust properties as well as other theoretical models that assume dust in thermal equilibrium at ~ 30 K that is well mixed with stars (e.g., Charlot & Fall 2000). To explain these observations, either the physical properties of the dust or the geometry of its spatial distribution have to change. In an upcoming paper, we will investigate this further by investigating in detail the dust temperature and its spatial distribution in high-redshift galaxies (Faisst et al., in prep).

The $R = 3000 - 4500$ Keck/DEIMOS optical spectra that are available for all 9 main galaxies⁵ allow us to investigate further the spectroscopical properties of the galaxies across the IRX– β diagram. The upper right panel of Figure 3 shows the IRX– β diagram with galaxies grouped in strong, weak, and no Ly α emitters. We do not see a trend with Ly α emission strength. The lower panel of Figure 3 shows median stacks of the spectra of galaxies with dust properties similar to the local starbursts (*HZ4*, *HZ9*, and *HZ10*) and galaxies below the SMC dust extinction curve. The spectra are binned to 1 Å and the 1σ uncertainties are derived by repeat-

ing the stacking analysis 500 times including Gaussian measurement uncertainties. This indicates that galaxies similar to local starbursts show deeper absorption in the Si II and Si IV doublet ISM lines at 1260 Å and 1400 Å, respectively, compared to galaxies below the SMC dust relation. Furthermore, there is indication of a flux deficit around N V (~ 1240 Å) and an upturn at 1225 Å. Such UV absorption features correlate well with the dust column density and gas-phase metallicity of galaxies (e.g., Heckman et al. 1998; Leitherer et al. 2011; Faisst et al. 2016b). Our findings therefore emphasize the diversity of galaxies at $z \sim 5.5$. Galaxies close to the local starburst relation are likely more evolved and metal-rich, while galaxies below the SMC relation that show weaker UV absorption features are dust-poor and metal-poor and possibly of younger age (see also Reddy et al. 2010). The latter is also suggested by estimates of the H α equivalent-width from the Spitzer colors of these galaxies (Faisst et al. 2017, in prep), indicating stellar populations of < 50 Myrs (e.g. Cowie et al. 2011). Importantly, these young galaxies can have substantially altered spatial dust distributions, which lead to the variety of UV spectral slopes at low IRX value. Specifically, clouds of dust may be expelled into the circum-galactic regions of these galaxies by interactions with their environment or internal radiation pressure and turbulences due to vigorous star formation. The serendipitous detections around *HZ8* and the quasar *HZ5* suggest a significant amount of circum-galactic material out to at least 10 kpc projected radius. *HZ5* has only a narrow Ly α emission (30 Å EW and 10 Å FWHM, Mallery et al. 2012) and its UV absorption features are at the same redshift as indicated by the [C II] emission of *HZ5a*. This is indicative of the UV undetected *HZ5a* absorbing a substantial part of the quasar’s light. *HZ8W* shows one of the reddest β but lowest IRX values which could hint toward a several kpc extended foreground dust screen of *HZ8*. *HZ10W* and the components of *HZ6* might be representatives of a similar situation. Future follow-up observations of these objects with JWST will be important to further study the inter-galactic medium around these galaxies.

5. CONCLUSION

We have obtained deep HST near-IR imaging to accurately measure the UV spectral slopes and luminosities of in total 14 $z \sim 5.5$ galaxies. We combine these new measurement with previous ALMA observations at 158 μ m available for all of these galaxies to investigate the IRX– β diagram at $z \sim 5.5$. The main findings and results of this letter are as follows:

- Our new HST observations greatly reduce the uncertainties and biases in UV spectral slopes compared to previous ground-based measurements.

⁵ We do not consider the low luminosity quasar *HZ5* here.

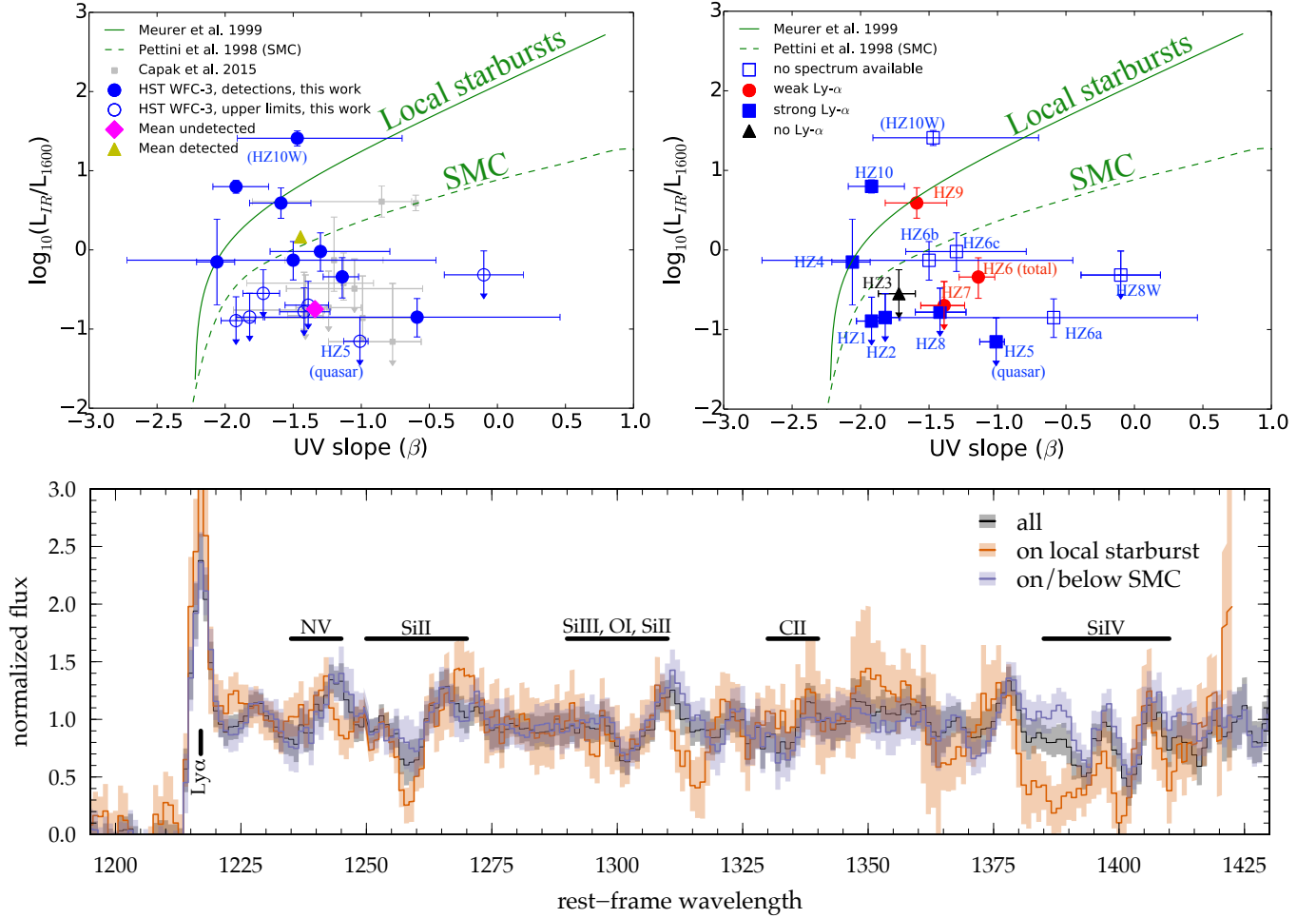


Figure 3. The IRX– β diagram and spectral properties of our $z \sim 5.5$ galaxies. *Upper left:* The blue symbols show updated β and L_{1600} measurements, and the mean values of detected (undetected) sources are shown with yellow (magenta) symbol. The previous measurement from C15 are shown by gray symbols. We also show relations from the literature, as indicated in the legend. *Upper right:* Galaxies color-coded according to their Ly α strength. We do not see a relation between Ly α emission and position on the IRX– β diagram. *Bottom:* Stacked Keck/DEIMOS spectra for galaxies falling on the local starburst relation (HZ4, HZ9, and HZ10; red) and below the SMC relation (blue). The black line shows all 9 galaxies (excluding the low-luminosity quasar HZ5). The 1σ uncertainties are indicated in colored bands.

Most of the galaxies at $z \sim 5.5$ are either consistent with local starbursts or dust properties similar to the SMC.

- The galaxies occupy a large range in IRX– β parameter space, indicative of a large diversity in their properties already 1 billion years after Big Bang.
- We find galaxies with low IRX values and large ranges of β , which cannot be explained by SMC-like dust nor models of well mixed stars and dust in thermal equilibrium. Instead the fundamental dust properties or the geometry of dust distribution has to change.
- Stacked rest-UV spectra of the galaxies across the

IRX– β diagram are indicative of a range of metallicities and evolutionary stages of the galaxies. In particular, galaxies close or below the SMC relation show weak UV absorption features indicative of a low dust and metal content.

We thank the anonymous referee for providing valuable feedback that helped to improve this work. D.R. and R.P. acknowledge support from the National Science Foundation under grant number AST-1614213 to Cornell University. R.P. acknowledges support through award SOSPA3-008 from the NRAO. V.S. acknowledges support from the European Union’s Seventh Framework program under grant agreement 337595 (ERC Starting Grant, ‘CoSMass’). Based on observations

made with the NASA/ESA Hubble Space Telescope, obtained [from the Data Archive] at the Space Telescope Science Institute, which is operated by the Association of Universities for Research in Astronomy, Inc., under NASA contract NAS 5-26555. These observations are associated with program #13641 and #13384. Some of the data presented herein were obtained at the W.M. Keck Observatory, which is operated as a scientific partnership among the California Institute of Technology, the University of California and the National Aeronautics and Space Administration. The Observatory was made possible by the generous financial support of the W.M. Keck Foundation. The authors wish to recognize and acknowledge the very significant cultural role and reverence that the summit of Mauna Kea has always

had within the indigenous Hawaiian community. We are most fortunate to have the opportunity to conduct observations from this mountain. This paper makes use of the following ALMA data: ADS/JAO.ALMA#2012.1.00523.S. ALMA is a partnership of ESO (representing its member states), NSF (USA) and NINS (Japan), together with NRC (Canada), NSC and ASIAA (Taiwan), and KASI (Republic of Korea), in cooperation with the Republic of Chile. The Joint ALMA Observatory is operated by ESO, AUI/NRAO and NAOJ. This research has made use of the NASA/IPAC Infrared Science Archive, which is operated by the Jet Propulsion Laboratory, California Institute of Technology, under contract with the National Aeronautics and Space Administration.

REFERENCES

- Bertin, E., & Arnouts, S. 1996, *A&AS*, 117, 393
- Bouwens, R. J., Illingworth, G. D., Oesch, P. A., et al. 2012, *ApJ*, 754, 83
- . 2014, *ApJ*, 793, 115
- Bouwens, R. J., Aravena, M., Decarli, R., et al. 2016, *ApJ*, 833, 72
- Capak, P. L., Riechers, D., Scoville, N. Z., et al. 2011, *Nature*, 470, 233
- Capak, P. L., Carilli, C., Jones, G., et al. 2015, *Nature*, 522, 455
- Carilli, C. L., & Walter, F. 2013, *ARA&A*, 51, 105
- Carilli, C. L., Chluba, J., Decarli, R., et al. 2016, *ApJ*, 833, 73
- Casey, C. M., Scoville, N. Z., Sanders, D. B., et al. 2014, *ApJ*, 796, 95
- Charlot, S., & Fall, S. M. 2000, *ApJ*, 539, 718
- Cowie, L. L., Barger, A. J., & Hu, E. M. 2011, *ApJ*, 738, 136
- de Barros, S., Schaerer, D., & Stark, D. P. 2014, *A&A*, 563, A81
- Dunlop, J. S., McLure, R. J., Robertson, B. E., et al. 2012, *MNRAS*, 420, 901
- Dunlop, J. S., McLure, R. J., Biggs, A. D., et al. 2017, *MNRAS*, 466, 861
- Faber, S. M., Phillips, A. C., Kibrick, R. I., et al. 2003, in *Proc. SPIE*, Vol. 4841, *Instrument Design and Performance for Optical/Infrared Ground-based Telescopes*, ed. M. Iye & A. F. M. Moorwood, 1657–1669
- Faisst, A. L. 2016, *ApJ*, 829, 99
- Faisst, A. L., Capak, P., Hsieh, B. C., et al. 2016a, *ApJ*, 821, 122
- Faisst, A. L., Capak, P. L., Davidzon, I., et al. 2016b, *ApJ*, 822, 29
- Finkelstein, S. L., Papovich, C., Salmon, B., et al. 2012, *ApJ*, 756, 164
- Genzel, R., Tacconi, L. J., Lutz, D., et al. 2015, *ApJ*, 800, 20
- Heckman, T. M., Robert, C., Leitherer, C., Garnett, D. R., & van der Rydt, F. 1998, *ApJ*, 503, 646
- Jiang, L., Finlator, K., Cohen, S. H., et al. 2016, *ApJ*, 816, 16
- Knudsen, K. K., Richard, J., Kneib, J.-P., et al. 2016, *MNRAS*, 462, L6
- Kong, X., Charlot, S., Brinchmann, J., & Fall, S. M. 2004, *MNRAS*, 349, 769
- Laigle, C., McCracken, H. J., Ilbert, O., et al. 2016, *ApJS*, 224, 24
- Leitherer, C., Tremonti, C. A., Heckman, T. M., & Calzetti, D. 2011, *AJ*, 141, 37
- Maiolino, R., Carniani, S., Fontana, A., et al. 2015, *MNRAS*, 452, 54
- Mallery, R. P., Mobasher, B., Capak, P., et al. 2012, *The Astrophysical Journal*, 760, 128
- Masters, D., Faisst, A., & Capak, P. 2016, *ApJ*, 828, 18
- Meurer, G. R., Heckman, T. M., & Calzetti, D. 1999, *ApJ*, 521, 64
- Oke, J. B. 1974, *ApJS*, 27, 21
- Pavesi, R., Riechers, D. A., Capak, P. L., et al. 2016, *ApJ*, 832, 151
- Peng, C. Y., Ho, L. C., Impey, C. D., & Rix, H.-W. 2010, *AJ*, 139, 2097
- Pettini, M., Kellogg, M., Steidel, C. C., et al. 1998, *ApJ*, 508, 539
- Reddy, N. A., Erb, D. K., Pettini, M., Steidel, C. C., & Shapley, A. E. 2010, *ApJ*, 712, 1070
- Riechers, D. A., Carilli, C. L., Capak, P. L., et al. 2014, *ApJ*, 796, 84
- Rogers, A. B., McLure, R. J., & Dunlop, J. S. 2013, *MNRAS*, 429, 2456
- Schaerer, D., Boone, F., Zamojski, M., et al. 2015, *A&A*, 574, A19
- Scoville, N., Aussel, H., Brusa, M., et al. 2007, *ApJS*, 172, 1
- Scoville, N., Sheth, K., Aussel, H., et al. 2016, *ApJ*, 820, 83
- Silverman, J. D., Daddi, E., Rodighiero, G., et al. 2015, *ApJL*, 812, L23
- Steidel, C. C., Rudie, G. C., Strom, A. L., et al. 2014, *ApJ*, 795, 165
- Watson, D., Christensen, L., Knudsen, K. K., et al. 2015, *Nature*, 519, 327